Biomech Model Mechanobiol (2008) 7:487–495
DOI 10.1007/s10237-007-0111-0

ORIGINAL PAPER

Interstitial fluid flow in the osteon with spatial gradients of mechanical properties: a finite element study

Agnès Rémond · Salah Naïli · Thibault Lemaire

Received: 16 November 2006 / Accepted: 22 October 2007 / Published online: 8 November 2007

Abstract Bone remodelling is the process that maintains bone structure and strength through adaptation of bone tissue mechanical properties to applied loads. Bone can be modelled as a porous deformable material whose pores are filled with cells, organic material and interstitial fluid. Fluid flow is believed to play a role in the mechanotransduction of signals for bone remodelling. In this work, an osteon, the elementary unit of cortical bone, is idealized as a hollow cylinder made of a deformable porous matrix saturated with an interstitial fluid. We use Biot's poroelasticity theory to model the mechanical behaviour of bone tissue taking into account transverse isotropic mechanical properties. A finite element poroelastic model is developed in the COMSOL Multiphysics software. Elasticity equations and Darcy's law are implemented in this software; they are coupled through the introduction of an interaction term to obtain poroelasticity equations. Using numerical simulations, the investigation of the effect of spatial gradients of permeability or Poisson's ratio is performed. Results are discussed for their implication on fluid flow in osteons: (i) a permeability gradient affects more the fluid pressure than the velocity profile; (ii) focusing on the fluid flow, the key element of loading is the strain rate; (iii) a Poisson's ratio gradient affects both fluid pressure and fluid velocity. The influence of textural and mechanical properties of bone on mechanotransduction signals for bone remodelling is also discussed.

Keywords Poroelasticity · Transverse isotropy · Compact bone · Osteon

A. Rémond · S. Naïli (✉) · T. Lemaire
Laboratoire de Mécanique Physique, UMR CNRS 7052 B2OA,
Faculté des Sciences et Technologie,
Université Paris XII-Val de Marne,
61 Avenue du Général de Gaulle,
94010 Créteil Cédex, France
e-mail: naili@univ-paris12.fr

A. Rémond
e-mail: a.remond@univ-paris12.fr

T. Lemaire
e-mail: lemaire@univ-paris12.fr

1 Introduction

Bone remodelling is the phenomenon that maintains and adapts bone structure to applied mechanical loading (Cowin 2001). Mechanical loading influences the rate of bone tissue renewal (Lanyon and Rubin 1984). It is important to link bone mechanical loading to local bone tissue remodelling since it could help to understand this latter phenomenon. From a mechanical point of view, cortical bone tissue can be seen as a multiscale deformable porous material, and an osteon as its basic structure unit (Cowin 2001; Martin et al. 1998). *Stimuli* for bone adaptation have been hypothesized to be shear stresses on cells membranes induced by interstitial fluid flow in the lacuno-canalicular porosity of the osteon (Weinbaum et al. 1994). Note that this hypothesis is now argued about in the literature (You et al. 2001). Thus mechanical loading's influence on fluid flow needs to be better understood. Since experimental work at this scale does not seem feasible at the moment, models have been developed (Smit et al. 2002; Steck et al. 2000; Weinbaum et al. 1994; Zeng et al. 1994; Zhang and Cowin 1994).

Models of the osteon permit to better understand the fluid–solid interaction for this type of tissue. Weinbaum et al. (1994) built a multiscale poroelastic model to explain how fluid shear stresses can act on bones cells to stimulate bone remodelling. Zhang and Cowin (1994) gave the closed-form solution of a cyclic loaded poroelastic beam, although this solution cannot be transposed to the cylindrical geometry of

the osteon. Note that both calculations of the pore pressure for a cylindrical structure and a beam have been compared (Zhang et al. 1998). Furthermore in both cases, material isotropy of the tissue was supposed in spite of the different mechanical properties in longitudinal and radial directions (Turner et al. 1999). The analytical solution for the pressure term obtained by Wang et al. (2000) was also used to study tracers concentrations within bone pores. They showed that permeability and loading frequency are key parameters of fluid transport. More recently, Rémond and Naili (2004) suggested a model of an osteon in which transverse isotropic mechanical properties have been taken into account.

Finite element method has been applied to solve poroelastic problems. Some softwares contain a poroelastic mode that can be used to model poroelastic material. Application to bone tissue was studied by Manfredini et al. (1999). They compared the analytical solution of the problem solved by Zhang and Cowin (1994) to the finite element one obtained with the Abaqus software for a rectangular beam of trabecular bone.

The aim of this work is to study macroscopic averaged flow and the way it is driven by mechanical loading at the osteon scale, including the effect of spatial gradients of mechanical properties. Indeed, as suggested by many references, cortical bone properties such as permeability or Poisson's ratio can vary spatially. For instance, physiological observations show that lacunae are more connected by canaliculi in the inner layers of osteons (You et al. 2004; Beno et al. 2006). Thus, the permeability parameter certainly decreases in the radial direction of osteons. Moreover, a few studies propose an experimental determination of Poisson's ratio of cortical bone and show that this parameter can vary. For instance, Reilly and Burstein (1975) assumed transverse isotropy of fibro-lamellar bone, and used extensometers to measure strains in two orthogonal directions concurrently. They found that the transverse and longitudinal Poisson's ratio values are bounded by 0.29 and 0.63. Ashman et al. (1984) reported on the use of an ultrasonic continuous wave technique, and found Poisson's ratio values ranging between 0.27 and 0.45. Pithioux et al. (2002) also used an ultrasonic method, and found that the Poisson's ratio varies between 0.12 and 0.29. More recently, Shahar et al. (2007) carried out an optical determination of this parameter ranging between 0.09 and 0.19. This dispersion of the values cannot only be explained by disparities between the different experimental techniques, but also by the microstructural differences that exist within various types of cortical bone (Turner et al. 1999; Zysset et al. 1999; Hengsberger et al. 2003).

When working with spatially varying mechanical properties, it is necessary to obtain a numerical solution to the poroelastic problem. An original method is used where linear elasticity equations and Darcy's law are coupled to obtain the poroelasticity model. A one-level porosity model based on cylindrical geometry of the osteon is developed. Its material properties are taken to be transverse isotropic. Both fluid and solid phases are supposed to be compressible. A cyclic longitudinal loading is applied. Then, using a finite element method, the influence of different mechanical parameters and their spatial variations are assessed.

After this introduction, the general formulation of the osteon model is given in Sect. 2. The method uses an original numerical approach based on a finite element method which is described in Sect. 3. Results and their implications on the interstitial fluid flow in the osteon are discussed in Sect. 4. Our attention particularly focuses on the effect of spatial gradients of mechanical properties. Thus the role of the permeability and Poisson's ratio are analyzed. Consequences of such spatial variations of mechanical parameters on mechanotransduction of bone's remodelling are finally discussed in Sect. 5.

2 General formulation

Poroelasticity theory (Biot 1955) is used to account for fluid–solid interactions in this model of an osteon. After describing the geometry and stating the main poroelasticity equations, boundary and initial conditions are specified.

2.1 Model's definition

A complete osteon is idealized as a hollow cylinder whose longitudinal axis is defined by $\mathbf{z}$, where $\mathbf{z}$ is a unit vector. The geometry is axisymmetric. The central hole models the Haversian canal through which interstitial fluid and blood flow. Inside and outside osteon radii are designated by r_i and r_o respectively. The height of the osteon is noted h. Cylindrical coordinates are (r, θ, z). Taking into account the axial symmetry, the problem depends only on coordinates r and z. The local basis associated with the cylindrical coordinates is a set of orthogonal unit vectors $(\mathbf{e}_r, \mathbf{e}_\theta, \mathbf{z})$.

2.2 Governing equations

Osteon tissue is considered as a deformable porous material saturated by an interstitial fluid phase. Poroelasticity theory (Biot 1955) is used to describe the mechanical behaviour of the osteon.

Mass conservation of the fluid phase The mass conservation law links the fluid content variation per unit volume ξ (dimensionless variable) in a given space to the fluid velocity vector $\mathbf{v}$:

$$\frac{\partial \xi}{\partial t} + \mathtt{div}\,\mathbf{v} = 0, \tag{1}$$

where div is the divergence operator. Time is denoted by t and the derivative with respect to t is written $\partial\square/\partial t$.

Momentum conservation equation Only low frequencies of loading occur for a large number of physiological activities except shocks. Thus, inertia terms are neglected in linear momentum conservation equation. No body forces are considered. In this case, the momentum conservation equation becomes:

$$\mathtt{div}\,\boldsymbol{\sigma} = \mathbf{0}, \tag{2}$$

where $\boldsymbol{\sigma}$ is the total stress tensor and div designates the usual divergence operator acting on a second-order tensor.

Constitutive equations are needed to complete the mechanical description of the osteon. The conjugated pairs of stress measures and strain measures are linked through linear relationships. These are specified in the following section.

Stress tensor constitutive relationship The stress tensor $\boldsymbol{\sigma}$ is linearly related to the skeleton strains $\boldsymbol{\epsilon}$ of the porous solid and to the fluid pressure p. This relationship is given by:

$$\boldsymbol{\sigma} = \mathbb{C}\boldsymbol{\epsilon} - \boldsymbol{\alpha}\, p, \tag{3}$$

where $\mathbb{C}$ is the drained stiffness fourth order tensor and $\boldsymbol{\alpha}$ is the Biot coefficients second-order tensor. These two tensors are assumed to be isotropic transverse with aligned principal directions.

The elastic porous material is transverse isotropic with its symmetry axis defined by $\mathbf{z}$. The drained stiffness tensor $\mathbb{C}$ is expressed in terms of five independent parameters, namely longitudinal Young's modulus E_z and Poisson's ratio ν_z, transverse Young's modulus E_r and Poisson's ratio ν_r, and longitudinal shear modulus G_z.

The diagonal Biot coefficients tensor $\boldsymbol{\alpha}$ is expressed in terms of two independent parameters α_r and α_z respectively in the $(\mathbf{e}_r, \mathbf{e}_\theta)$ isotropic plane and along the z-axis of symmetry.

The skeleton strain tensor $\boldsymbol{\epsilon}$ is related to the porous matrix displacement field $\mathbf{u}$ by the relationship:

$$\boldsymbol{\epsilon} = \frac{1}{2}\left(\mathtt{grad}\,\mathbf{u} + (\mathtt{grad}\,\mathbf{u})^{\mathrm{T}}\right), \tag{4}$$

where grad is the gradient operator acting on a vector field and the superscript $\square^{\mathrm{T}}$ designates the transpose operator.

Fluid content constitutive relationship This relationship gives the pore pressure p as a function of the variation in fluid content ξ and the strain $\boldsymbol{\epsilon}$. This constitutive relationship is defined by:

$$p = M\left\{\xi - \mathtt{Tra}\,(\boldsymbol{\alpha}\boldsymbol{\epsilon})\right\}, \tag{5}$$

where M is the Biot modulus and Tra is the trace operator.

Darcy's law Darcy's law is a linear relationship between the fluid velocity vector $\mathbf{v}$ and the pore pressure gradient. It is written:

$$\mathbf{v} = -K\,\mathtt{grad}\,p, \tag{6}$$

where grad is the gradient operator acting on a scalar field. The permeability $K = \kappa/\mu$ is defined by the ratio between the intrinsic permeability κ and the interstitial dynamic fluid viscosity μ.

Reformulated equations of poroelasticity Substituting the constitutive relationship (3) into the momentum conservation Eq. (2) leads to:

$$\mathtt{div}(\mathbb{C}\boldsymbol{\epsilon}) = \boldsymbol{\alpha}\,\mathtt{grad}\,p. \tag{7}$$

Furthermore, Darcy's law (6) and the fluid content constitutive relationship (5) are combined to the mass conservation Eq. (1) to give:

$$\frac{1}{M}\frac{\partial p}{\partial t} - \mathtt{div}(K\,\mathtt{grad}\,p) = -\frac{\partial}{\partial t}\left(\mathtt{Tra}(\boldsymbol{\alpha}\boldsymbol{\epsilon})\right). \tag{8}$$

These last two Eqs. (7) and (8) lead to a system of equations whose unknowns are the displacement vector $\mathbf{u}$ and the pore pressure p. In what follows, boundary and initial conditions for the problem are described.

2.3 Boundary and initial conditions

Boundary conditions Pressure inside the Haversian canal is used as a reference pressure. Considering the low frequencies of loading, this canal is large enough to hold the reservoir function. Its dimensions enable the fluid to relax so that its pressure can be assumed to remain constant. The exterior lateral surface of the osteon is supposed to be impermeable. Thus, there is no macroscopic fluid flow through this surface. Full impermeability is an idealization of the real boundary condition since a few canaliculi can cross this lateral surface (which is called cement surface) and thus enable the fluid to flow. In addition, bases of the hollow cylinder are assumed to be impermeable. As a consequence, the following boundary conditions for the pore pressure must be taken into account:

$$\begin{cases} p = 0, \ \forall\, r = r_i; \quad \mathtt{grad}\,p \cdot \mathbf{e}_r = 0, \ \forall\, r = r_o, \\ \mathtt{grad}\,p \cdot \mathbf{z} = 0, \ \forall\, z = 0; \quad \mathtt{grad}\,p \cdot \mathbf{z} = 0, \ \forall\, z = h. \end{cases} \tag{9}$$

Stresses on the Haversian canal surface are supposed to be negligible compared to stresses induced by the fluid flow. It leads to the boundary condition on stress:

$$\boldsymbol{\sigma}\,\mathbf{e}_r = \mathbf{0}, \quad \forall\, r = r_{\mathrm{i}}. \tag{10}$$

On the outside boundary at $r = r_o$, the radial displacement is constrained to zero. Cyclic loading in the longitudinal direction is applied. Applied loading results in the maximal

longitudinal displacement of magnitude $h\epsilon_0$ at a given f frequency, where ϵ_0 is the longitudinal strain amplitude. This latter condition is imposed on the longitudinal displacement field for $z = h$. In addition, the displacement is constrained to zero for $z = 0$. These conditions are given by the relationships:

$$\begin{cases} \mathbf{u} \cdot \mathbf{e}_r = 0, \ \forall r = r_o; \\ \mathbf{u} \cdot \mathbf{z} = 0, \ \forall z = 0; \quad \mathbf{u} \cdot \mathbf{z} = -\epsilon_0 h \sin ft, \ \forall z = h. \end{cases} \tag{11}$$

The condition imposed on $z = h$ via Eqs. (11) allows to obtain a periodic variation of the longitudinal displacement always equal to 2π for all frequencies.

Initial conditions The poroelastic material is supposed to be at rest at times $t < 0$.

3 Method of solution

COMSOL Multiphysics (2005), a finite element software for various multiphysical problems, was used. This software contains a library from which classical physical models can be combined. It can be used to solve coupled physics phenomena such as the poroelasticity as a combination of elasticity and Darcy's law.

3.1 Mesh

The axis $(O; \mathbf{z})$ defines the axisymmetry axis for the geometrical model. Thus, the plane $(O; \mathbf{e}_r, \mathbf{z})$ for the positive radii is enough to describe the problem. This plane is meshed, however one should keep in mind that the value calculated at each node is the value on a circle for the hollow cylinder model. Similarly, each element represents the cross section of an annulus. A rectangle of dimension $(r_o - r_i) \times h = 100 \times 1{,}000\ \mu m^2$ is meshed with a total of 75 quadrangle elements, since the geometry is regular enough. The finite elements are of quadratic lagrange type. This choice is made to ensure continuity of pressure gradients, since they are included in the interaction term.

3.2 Computations

Poroelasticity equations were solved as coupled elasticity and Darcy's law problems. The interaction between fluid flow and solid matrix deformations is given by external forces in elasticity and source terms in Darcy's law mode. Poroelasticity equations are implemented in the software COMSOL Multiphysics. Equations are then solved simultaneously in the time-domain to calculate the response of the system to cyclical load.

Table 1 Material properties used in the poroelastic model of the osteon

E_r	17 GPa	E_z	12 GPa
ν_r	0.3	ν_z	0.3
G_z	9 GPa		
M	40 GPa		
α_r	0.15	α_z	0.15
κ	10^{-18} m^2	μ	10^{-3} Pa s

3.3 Parameters for the computations

The computation of the system response is based on a direct time integration scheme. The time step must be chosen to ensure accuracy and stability requirements. Time step is kept under a critical value calculated from loading frequency. In order to improve the stability, Rayleigh's damping was added to the elasticity equations in the numerical scheme. Comparison with the analytical solution developed by Rémond and Naili (2005b) showed that damping did not influence numerical results (Rémond and Naili 2005a).

Using material properties of cortical bone listed in Table 1, the solution to the poroelastic problem is computed with values adapted from the literature and for osteon's inside and outside radii being $r_i = 50\ \mu m$ and $r_o = 150\ \mu m$ respectively (Cowin 2001).

According to boundary condition (11), results are computed for loading conditions defined by a loading frequency f and a longitudinal strain amplitude ϵ_0. Two types of simulations are proposed which are described in the following paragraph.

Influence of permeability Permeability can be seen as the macroscopic indicator of the fluid flow at the microscopic level. According to recent results of Beno et al. (2006), this parameter lies between 10^{-23} and 10^{-18} m^2. Nevertheless, the low values of this parameter seem too small to suit with continuum mechanics. That is why we choose to work with the largest value proposed by these authors, considering a reference case with a constant permeability of $\kappa = 10^{-18}$ m^2. Since this parameter is only estimated, its spatial variations are difficult to quantify. There seems to be fewer canaliculi connecting lacunae toward the exterior of the osteon, which would lead to a decreasing permeability from the inside radius to the outside one (Cowin 2001). To study the influence of its variations, Poisson's ratio is kept constant ($\nu_r = 0.3$) and the permeability is assumed to be a linear function between r_i and r_o. For this purpose, three cases are considered: Case 1 ($\kappa_i = 10^{-18}$ m^2 and $\kappa_o = 0.5 \times 10^{-18}$ m^2); Case 2 ($\kappa_i = 10^{-18}$ m^2 and $\kappa_o = 0.1 \times 10^{-18}$ m^2); Case 3 ($\kappa_i = 2 \times 10^{-18}$ m^2 and $\kappa_o = 10^{-18}$ m^2) where the permeability is noted κ_i at r_i and κ_o at r_o.

The role of loading frequency is also considered *via* two frequencies (1 and 20 Hz). By maintaining a constant longitudinal strain rate, it is possible to study the sensitivity of poroelastic behaviour of bone with mechanical properties gradients without taking into account the loading frequency influence. Thus, when textural or mechanical gradients are considered, these loading conditions are chosen so that the magnitude of the longitudinal strain rate $\dot{\epsilon} = \epsilon_0 f$ can remain constant, setting $\dot{\epsilon} = 10^{-3}$ Hz. This value can be compared with bone remodelling mechanotransduction signals (Turner 1998; Burger et al. 2003) which are bounded by 10^{-4} and 10^{-3} Hz.

Influence of Poisson's ratio This coefficient is the matrix material parameter that links loading in one direction to deformation in another direction. Since fluid flow is driven by the porous solid matrix deformation through the interaction term, variations of solid porous matrix Poisson's ratio do affect pressure. The mechanical behaviour of the osteon depends on Poisson's ratio, its influence is studied by using a linear variation of ν_r between r_i and r_o. Its reference value is assumed to be defined by $\nu_r = 0.30$ (Cowin 1999). Considering a constant permeability of $10^{-18}\,\mathrm{m}^2$, two cases are considered: Case 1 ($\nu_\mathrm{i} = 0.15$ and $\nu_\mathrm{o} = 0.3$); Case 2 ($\nu_\mathrm{i} = 0.3$ and $\nu_\mathrm{o} = 0.45$) where Poisson's ratio ν_r is denoted by ν_i at r_i and ν_o at r_o.

Remarks Before presenting numerical results given by the present model, we must bear in mind that its validity has been checked comparing its steady state simulations with an analytical solution considering constant mechanical properties of the medium (Rémond and Naili 2005b). When spatial gradient of permeability or Poisson's ratio are considered, this closed-form solution is no longer valid and numerical calculations are required to obtain the poroelastic response of the osteon to cyclic load. In the next section, such numerical results are presented. To assess their validity, all the following results include a representative closed-form solution case with a constant permeability or Poisson's ratio ν_r.

4 Results

Results for pressure and fluid velocity distributions are presented in the following section. The typical loading frequency is chosen to be 1 Hz which corresponds to walking activity. Results for interstitial fluid pressure and fluid velocity in the radial direction of the osteon are exhibited at half the height of the osteon, i.e. at $z = h/2$, when the pressure peak is reached, i.e. when the maximal compression effect is observed.

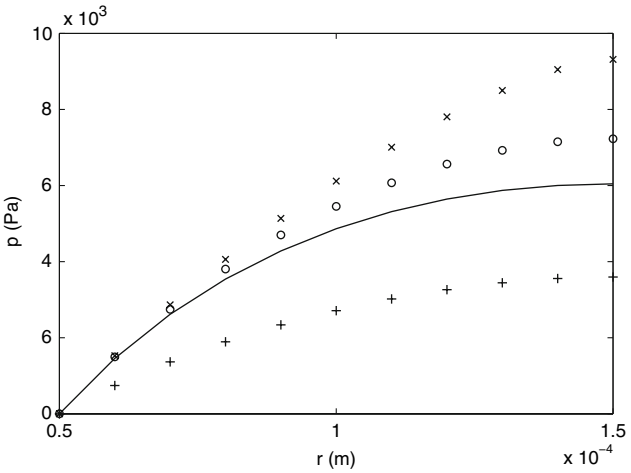

Fig. 1 The frequency of loading and longitudinal strain amplitude are fixed at $f = 1$ Hz and $\epsilon_0 = 1 \times 10^{-3}$ respectively. Pressure versus radial coordinate for linear variations of the permeability values: Case 1 ($\kappa_\mathrm{i} = 10^{-18}\,\mathrm{m}^2$ and $\kappa_\mathrm{o} = 0.5 \times 10^{-18}\,\mathrm{m}^2$) ($\circ\circ$); Case 2 ($\kappa_\mathrm{i} = 10^{-18}\,\mathrm{m}^2$ and $\kappa_\mathrm{o} = 0.1 \times 10^{-18}\,\mathrm{m}^2$) ($\times\times$); Case 3 ($\kappa_\mathrm{i} = 2 \times 10^{-18}\,\mathrm{m}^2$ and $\kappa_\mathrm{o} = 10^{-18}\,\mathrm{m}^2$) ($++$) and a constant permeability $\kappa = 10^{-18}\,\mathrm{m}^2$ (*solid line*)

4.1 Permeability spatial gradient

Pressure Results for pressure as a function of the osteon radius are shown on Fig. 1. The loading frequency and the longitudinal strain amplitude are respectively $f = 1$ Hz and $\epsilon_0 = 1 \times 10^{-3}$.

As shown on this figure, pressure builds up toward the outside radius. This trend can be linked to the non-leaking condition on the cement surface. Moreover, permeability gradients modify strongly the pressure profiles. For instance, taking as a reference a constant permeability (solid line), the relative variations for Cases 1 and 2, which are lower than 10% for radii smaller than 7×10^{-5} m, do increase to reach respectively 20 and 50% at the cement surface. The trend is different for Case 3 since the relative variation of pressure is more pronounced near the Haversian canal (about -45% at $r = 7 \times 10^{-5}$ m) than in the outer part of osteon (about -39% at the cement surface). It indicates that: (i) the permeability gradient quantitatively affects the pressure profile; (ii) compared to the value of its gradient, the value of the permeability at the inside radius plays a more important role on the development of the pressure peaks. This latter point is logical since the fluid flows from the Haversian canal to the cement line and is thus strongly dependent on the inflow-outflow conditions, that is to say on the value of the permeability at r_i.

Fluid velocity Fluid flow at the macroscopic scale is important since it represents the average fluid flow through the canaliculi and can be linked to fluid flow at the microscopic scale in the lacuno-canalicular porosity. Moreover, it

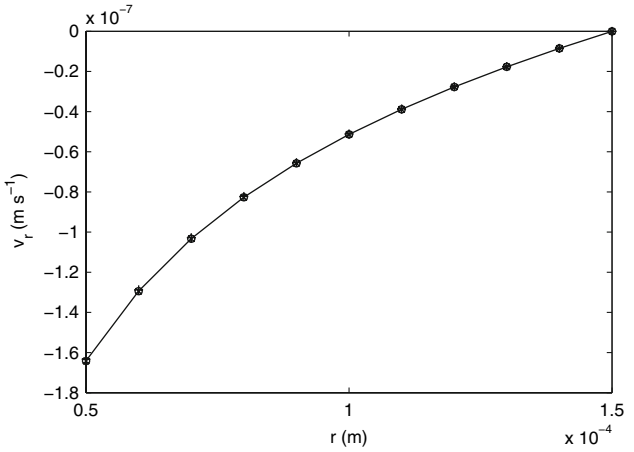

Fig. 2 The frequency of loading and longitudinal strain amplitude are fixed at $f = 1\,\text{Hz}$ and $\epsilon_0 = 1 \times 10^{-3}$ respectively. Radial fluid velocity versus radial coordinate for linear variations of the permeability values: Case 1 ($\kappa_\text{i} = 10^{-18}\,\text{m}^2$ and $\kappa_\text{o} = 0.5 \times 10^{-18}\,\text{m}^2$) (○○); Case 2 ($\kappa_\text{i} = 10^{-18}\,\text{m}^2$ and $\kappa_\text{o} = 0.1 \times 10^{-18}\,\text{m}^2$) (××); Case 3 ($\kappa_\text{i} = 2 \times 10^{-18}\,\text{m}^2$ and $\kappa_\text{o} = 10^{-18}\,\text{m}^2$) (++) and a constant permeability $\kappa = 10^{-18}\,\text{m}^2$ (*solid line*)

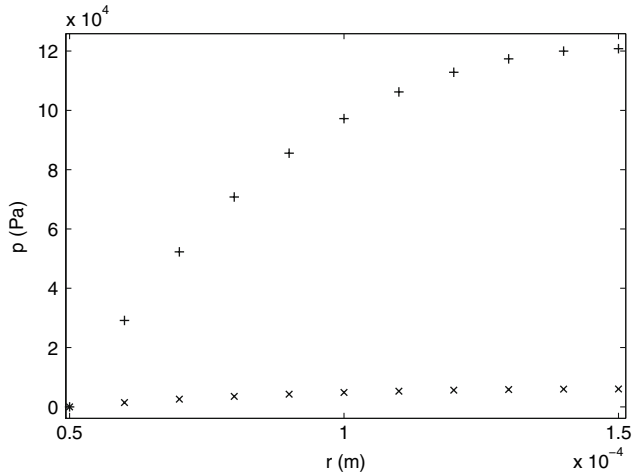

Fig. 3 The longitudinal strain amplitude is fixed at $\epsilon_0 = 1 \times 10^{-3}$. Pressure versus radial coordinate for constant permeability and Poisson's ratio values: (i) $f = 1\,\text{Hz}$ (××); (ii) $f = 20\,\text{Hz}$ (++)

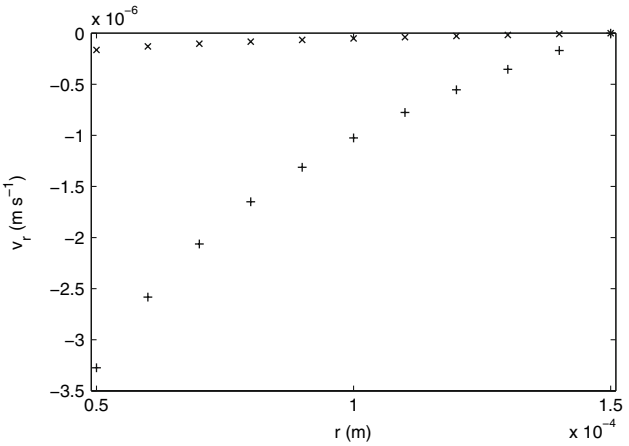

Fig. 4 The longitudinal strain amplitude is fixed at $\epsilon_0 = 1 \times 10^{-3}$. Radial velocity versus radial coordinate for constant permeability and Poisson's ratio values: (i) $f = 1\,\text{Hz}$ (××); (ii) $f = 20\,\text{Hz}$ (++)

is known that this interstitial flow is crucial in the mechanotransduction of signals of bone remodelling (Burger et al. 2003). Thus, the radial fluid velocity, obtained through the Darcy's law given by Eq. (6), is presented on Fig. 2 for the three cases of permeability variation with the same conditions as in the previous paragraph. This figure indicates that spatial gradients of the permeability do not lead to a notable variation of the radial fluid velocity distribution. This result shows that permeability variations are compensated by spatial pressure variations, having no significant consequences on the radial fluid velocity. To complete this study, we must analyse the possible role of loading frequency.

4.2 Loading frequency

In this paragraph, we intend to show the role of loading frequency. Two types of simulations are performed to do that. Firstly, two loading frequencies (1 and 20 Hz) are considered when $\kappa = 10^{-18}\,\text{m}^2$, $\nu_r = 0.3$ and $\epsilon_0 = 1 \times 10^{-3}$. The lower frequency corresponds to a walking activity while the higher one refers to a mechanical stimulation without any shock. With these parameters, the pressure and radial velocity fields developing along the osteon radius are evaluated. Secondly, the study proposed previously in Sect. 4.1 (paragraph Pressure) is done again keeping the same longitudinal strain rate $\dot{\epsilon}$ but considering a higher loading frequency $f = 20\,\text{Hz}$ and the corresponding strain amplitude $\epsilon_0 = 5 \times 10^{-5}$.

Study for a given longitudinal strain amplitude In order to assess the role of loading frequency, pressure and velocity profiles are plotted for a longitudinal strain amplitude $\epsilon_0 = 1 \times 10^{-3}$. Two levels of loading frequency are studied: (i) $f = 1\,\text{Hz}$ which typically corresponds to the frequency resulting from walking activity; (ii) $f = 20\,\text{Hz}$. Figure. 3 presents a comparison between pressure profiles at these two frequencies. The higher the frequency is, the more dramatically the pressure builds up toward the osteon radius. Similar results are visible on Fig. 4 since the fluid velocity corresponding to the higher frequency is one order of magnitude larger than the one corresponding to walking activity. These results show the strong dependency of the elastic response of bone on loading frequency as shown by (Wang et al. 2000; Rémond and Naili 2005a). Nevertheless, the key parameter governing the poroelastic response of the system is the longitudinal strain rate $\dot{\epsilon}$.

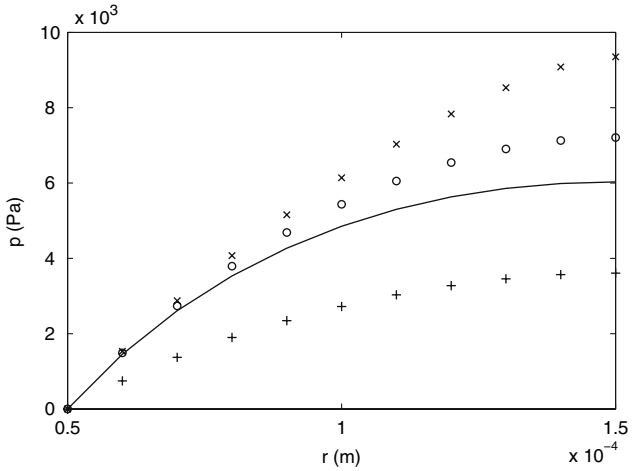

Fig. 5 The frequency of loading and longitudinal strain amplitude are fixed at $f = 20\,\text{Hz}$ and $\epsilon_0 = 5 \times 10^{-5}$ respectively. Pressure versus radial coordinate for linear variations of the permeability values: Case 1 ($\kappa_\text{i} = 10^{-18}\,\text{m}^2$ and $\kappa_\text{o} = 0.5 \times 10^{-18}\,\text{m}^2$) ($\circ\circ$); Case 2 ($\kappa_\text{i} = 10^{-18}\,\text{m}^2$ and $\kappa_\text{o} = 0.1 \times 10^{-18}\,\text{m}^2$) ($\times\times$); Case 3 ($\kappa_\text{i} = 2 \times 10^{-18}\,\text{m}^2$ and $\kappa_\text{o} = 10^{-18}\,\text{m}^2$) ($++$) and a constant permeability $\kappa = 10^{-18}\,\text{m}^2$ (*solid line*)

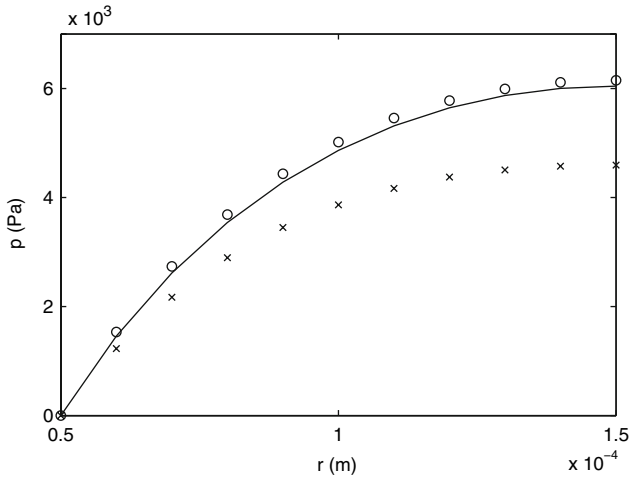

Fig. 6 The frequency of loading and longitudinal strain amplitude are fixed at $f = 1\,\text{Hz}$ and $\epsilon_0 = 1 \times 10^{-3}$ respectively. Pressure versus radial coordinate for linear variations of Poisson's ratio: Case 1 ($\nu_\text{i} = 0.15$ and $\nu_\text{o} = 0.3$) ($\circ\circ$); Case 2 ($\nu_\text{i} = 0.3$ and $\nu_\text{o} = 0.45$) ($\times\times$) and a constant Poisson's ratio $\nu_r = 0.30$ (*solid line*)

Study considering a constant longitudinal strain rate To check the crucial role of $\dot{\epsilon}$, the pressure profiles presented on Fig. 1 are calculated again for a higher loading frequency $f = 20\,\text{Hz}$ and the corresponding strain amplitude $\epsilon_0 = 5 \times 10^{-5}$, keeping the same longitudinal strain rate $\dot{\epsilon} = 10^{-3}\,\text{Hz}$. These results are presented on Fig. 5. These profiles are very close to those of Fig. 1. Thus, preserving the longitudinal strain rate $\dot{\epsilon}$, the role of the frequency remains very weak. Since the radial fluid velocity is calculated from these pressure profiles through the Darcy law (6), the radial velocities derived from Fig. 5 are very close to those of Fig. 2 and are not presented here.

Remarks The results obtained in this section involving spatial gradients of the permeability show that when permeability varies, interstitial fluid flow is not affected as much as pressure peak values. This can be explained since fluid flow is driven through the quasi-uniform deformation of the porous matrix resulting from longitudinal loading. Thus, interstitial fluid flow leads to higher pressure values when permeability decreases toward the outside radius. These results show that the solid matrix deformation drives fluid flow because the imposed mechanical loading is introduced through the longitudinal deformation of the porous matrix. It is necessary to complete this study by analyzing the influence of Poisson's ratio spatial gradient since this coefficient plays an important role in the interaction between matrix deformation and fluid flow.

4.3 Poisson's ratio spatial gradient

Considering the loading conditions used to obtain the results drawn on Figs. 1 and 2, profiles of pressure and radial velocity are plotted for a constant permeability ($\kappa = 10^{-18}\,\text{m}^2$) and spatial gradients of Poisson's ratio. The two considered cases are: Case 1 ($\nu_\text{i} = 0.15$ and $\nu_\text{o} = 0.3$); Case 2 ($\nu_\text{i} = 0.3$ and $\nu_\text{o} = 0.45$) where Poisson's ratio is denoted by ν_i at r_i and ν_o at r_o by using a linear variation of ν_r between r_i and r_o. Moreover, the reference case with a constant Poisson's ratio of $\nu_r = 0.3$ is also presented.

Pressure As shown on Fig. 6, the pressure profiles that develop radially depend on Poisson's gradient. We consider a Poisson's ratio of $\nu_r = 0.3$ as the reference. In Case 1, Poisson's ratio becomes larger than the reference value toward the outside radius, which would correspond to a more compressible porous solid matrix at the radius r_i, pressure builds up to a larger value than the reference value with a constant Poisson's ratio. On the other hand, if the porous matrix is considered as more compressible than the porous matrix reference toward the zone of the Haversian canal, pressure remains significantly lower for the same loading.

Fluid velocity Figure 7 presents the corresponding radial fluid velocity derived from previous pressure profiles. The radial flow is modified when Poisson's ratio spatially changes. Quantitatively, these changes are the same as those described in the previous paragraph therefore similar conclusions can be drawn. Thus, in the first case, the radial velocity profile remains close to the reference curve whereas in the second case, it is higher.

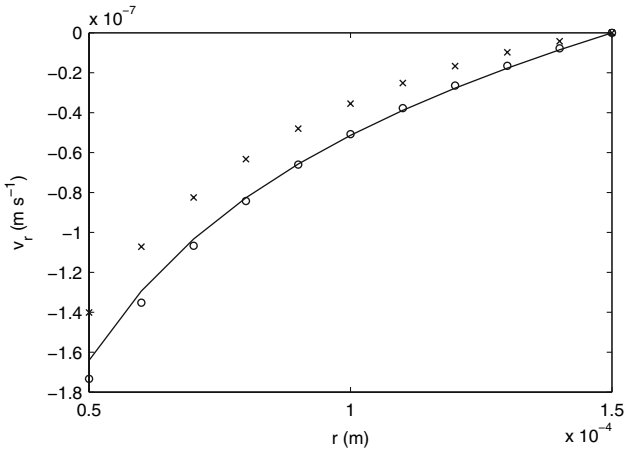

Fig. 7 The frequency of loading and longitudinal strain amplitude are fixed at $f = 1$ Hz and $\epsilon_0 = 1 \times 10^{-3}$. Radial fluid velocity versus radial coordinate for linear variations of Poisson's ratio: Case 1 ($\nu_i = 0.15$ and $\nu_o = 0.3$) (○○); Case 2 ($\nu_i = 0.3$ and $\nu_o = 0.45$) (××) and a constant Poisson's ratio $\nu_r = 0.30$ (*solid line*)

Since these results were computed for values relevant to a model of an osteon, possible implications of these findings are discussed in the following section.

5 Discussion and conclusion

5.1 Relevance to mechanotransduction

Mechanotransduction signals for bone remodelling are linked to fluid flow (Burger et al. 2003). Cells buried in the lacuna-canalicular porosity of the bone matrix have shown sensitivity to shear stresses induced by fluid flow. Since it was also observed that bone had maintained and increased its mass density when cyclically loaded (Lanyon 1984; Qin et al. 2002); models have been developed to link these phenomena and to explain part of the bone tissue behaviour. At the osteon scale, the present model allows us to study the influence of mechanical loading on fluid flow. The mechanical adaptation of bone suggests that this system senses the applied mechanical loading. It transmits the loading information to cells. These cells respond through bone tissue resorption and apposition. Therefore, bone tissue adapts to the applied mechanical loading.

Influence of the permeability spatial gradient Simulations proposed to analyze the influence of permeability spatial gradient suggest that pressure is strongly affected by textural variations whereas fluid velocity is not. Indeed the pressure peaks at a higher value when permeability decreases toward the outside of the osteon. This phenomenon develops to maintain a similar radial fluid velocity. Thus, at the osteon scale, since permeability changes do not modify significantly the interstitial fluid flow, the cell sensitivity to this parameter is certainly less important than *a priori* expected. However, there is a limit to this conclusion; since the calculated velocity is averaged information, the present results should be scaled down to estimate effects at the cell scale. This macroscopic approach does not allow us to represent narrowing or clogging effects located at the pore scale, and the resulting microscopic friction effects are washed out through the macroscopic permeability parameter.

Permeability is not directly linked to variations of fluid velocity within the osteon but gives an indication of pressure peaks. According to recent studies suggesting that pressure could also influence bone cell behaviour (Nagatomi et al. 2001, 2002), gradients of permeability play a more important role in cell response through pressure than fluid velocity.

Furthermore, these results show that we must focus on in the inflow–outflow area, that is to say near the Haversian canal since the hydraulic response across osteon is very sensitive to the value of permeability at $r = r_i$.

Influence of Poisson's ratio spatial gradient Similarly, since the porous matrix elastic properties of the osteon vary spatially (Martin et al. 1998), influence of Poisson's ratio spatial gradient has been investigated. Our results show that both pressure and radial fluid velocity are influenced by spatial gradients of Poisson's ratio alike. Consequently, mechanotransduction signals discussed above are directly affected by spatial gradients of this poroelastic parameter which is directly linked with aging effects, mineralization, etc. (Cowin 2001).

5.2 Conclusion and perspectives

Finite element analysis using a coupled physics mode in software COMSOL Multiphysics has been developed to solve poroelastic problems applied to osteon. Comparison with steady state closed-form solution showed that this method can accurately solve equations for a poroelastic problem. Results presented here show how relevant it can be to account for textural and elastic spatial gradients since they do influence hydraulic response of the osteon. Consequently, such variations in mechanical properties of bone result in different mechanotransduction signals for bone cells. This work also leads naturally to the question of temporal variations of these properties when the osteon is formed and that could lead to supplementary differences especially in the longitudinal direction (Martin et al. 1998).

References

Ashman RB, Cowin SC, Van Buskirk WC, Rice JC (1984) A continuous wave technique for the measurement of the elastic properties of cortical bone. J Biomech 17:349–361

Beno T, Yoon Y-J, Cowin SC, Fritton SP (2006) Estimation of bone permeability using accurate microstructural measurements. J Biomech 39:2378–2387

Biot MA (1955) Theory of elasticity and consolidation for a porous anisotropic solid. J Appl Phys 26(2):182–185

Burger EH, Klein-Nulend J, Smit TH (2003) Strain-derived canalicular fluid flow regulates osteoclast activity in a remodelling osteon–a proposal. J Biomech 36(10):1453–1459

COMSOL Multiphysics (2005) Model library. Grenoble, France

Cowin SC (1999) Bone poroelasticity. J Biomech 32:217–238

Cowin SC (2001) Bone mechanics handbook, 2nd edn. CRC Press, Boca Raton

Hengsberger S, Enstroem J, Peyrin F, Zysset P (2003) How is the indentation modulus of bone tissue related to its macroscopic elastic response? A validation study. J Biomech 36(10):1503–1509

Lanyon LE (1984) Functional strain as a determinant for bone remodeling. Calcif Tissue Int 36(Suppl 1):S56–S61

Lanyon LE, Rubin CT (1984) Static vs dynamic loads as an influence on bone remodelling. J Biomech 17(12):897–905

Manfredini P, Cocchetti G, Maier G, Redaelli A, Montevecchi FM (1999) Poroelastic finite element analysis of a bone specimen under cyclic loading. J Biomech 32(2):135–144

Martin RB, Burr DB, Sharkey NA (1998) Skeletal tissue mechanics, 1st edn. Springer, New York

Nagatomi J, Arulanandam BP, Metzger DW, Meunier A, Bizios R (2001) Frequency- and duration-dependent effects of cyclic pressure on select bone cell functions. Tissue Eng 7(6):717–728

Nagatomi J, Arulanandam BP, Metzger DW, Meunier A, Bizios R (2002) Effects of cyclic pressure on bone marrow cell cultures. J Biomech Eng 124(3):308–314

Pithioux M, Lasaygues P, Chabrand P (2002) An alternative method to determine the elastic properties of cortical bone. J Biomech 35:961–968

Qin YX, Lin W, Rubin C (2002) The pathway of bone fluid flow as defined by in vivo intramedullary pressure and streaming potential measurements. Ann Biomed Eng 30(5):693–702

Reilly D, Burstein A (1975) The elastic and ultimate properties of compact bone tissue. J Biomech 8:393–405

Rémond A, Naili S (2004) Cyclic loading of a transverse isotropic poroelastic cylinder: a model for the osteon. Comptes Rendus Mecanique 332(9):759–766

Rémond A, Naili S (2005a) Finite element analysis of a poroelastic model: application to an osteon under cyclic loading. Proc 4th ICCHMT II:1080–1084

Rémond A, Naili S (2005b) Transverse isotropic poroelastic osteon model under cyclic loading. Mech Res Commun 32(6):645–651

Shahar R, Zaslansky P, Barak M, Friesem AA, Currey JD, Weiner S (2007) Anisotropic poisson's ratio and compression modulus of cortical bone determined by speckle interferometry. J Biomech 340:252–264

Smit TH, Huyghe JM, Cowin SC (2002) Estimation of the poroelastic parameters of cortical bone. J Biomech 35(6):829–835

Steck R, Niederer P, Knothe Tate ML (2000) A finite difference model of load-induced fluid displacements within bone under mechanical loading. Med Eng Phys 22(2):117–125

Turner CH (1998) Three rules for bone adaptation to mechanical *stimuli*. Bone 23(5):399–407

Turner CH, Rho J, Takano Y, Tsui TY, Pharr GM (1999) The elastic properties of trabecular and cortical bone tissues are similar: results from two microscopic measurement techniques. J Biomech 32(4):437–441

Wang L, Cowin SC, Weinbaum S, Fritton SP (2000) Modeling tracer transport in an osteon under cyclic loading. Ann Biomed Eng 28(10):1200–1209

Weinbaum S, Cowin SC, Zeng Y (1994) A model for the excitation of osteocytes by mechanical loading-induced bone fluid shear stresses. J Biomech 27(3):339–360

You L, Cowin SC, Schaffler MB, Weinbaum S (2001) A model for strain amplification in the actin cytoskeleton of osteocytes due to fluid drag on pericellular matrix. J Biomech 34(11):1375–1386

You LD, Weinbaum S, Cowin SC, Schaffler MB (2004) Ultrastructure of the osteocyte process and its pericellular matrix. Anat Rec 278A(2):505–513

Zeng Y, Cowin SC, Weinbaum S (1994) A fiber matrix model for fluid flow and streaming potentials in the canaliculi of an osteon. Ann Biomed Eng 22(3):280–292

Zhang D, Cowin SC (1994) Oscillatory bending of a poroelastic beam. J Mech Phys Solids 42(10):1575–1599

Zhang D, Weinbaum S, Cowin SC (1998) On the calculation of bone pore water pressure due to mechanical loading. Int J Solids Struct 35(34-35):4981–4997

Zysset PK, Guo XE, Hoffler CE, Moore KE, Goldstein SA (1999) Elastic modulus and hardness of cortical and trabecular bone lamellae measured by nanoindentation in the human femur. J Biomech 32(10):1005–1012